forests

MDPI

Communication

Nucleation Process of the 2017 Nuugaatsiaq, Greenland Landslide

Zhenwei Guo [1,2,3], Xinrong Hou [1,2,3], Dawei Gao [1,2,3,*] and Jianxin Liu [1,2,3]

[1] Key Laboratory of Metallogenic Prediction of Nonferrous Metals and Geological Environment Monitoring, Ministry of Education, Changsha 410083, China
[2] Key Laboratory of Non-Ferrous Resources and Geological Hazard Detection, Changsha 410083, China
[3] School of Geosciences and Info-Physics, Central South University, Changsha 410083, China
* Correspondence: daweigao@csu.edu.cn

Abstract: Seismic precursors prior to the failure of rocks are essential for probing the nucleation process and mitigating hazards. However, such precursory events before large landslides are rarely reported possibly due to the lack of near-source observations. The 2017 Nuugaatsiaq, Greenland landslide that was preceded by an abundance of small earthquakes and captured by a local seismic station is a notable exception and offers us a valuable opportunity to investigate how a large landslide initiated. Prior work suggests that accelerated creeping plays an important role during the landslide nucleation process. However, by analyzing the temporal evolution of the waveform similarities, waveform amplitudes, and inter-event times of the seismic precursors, we find that the Nuugaatsiaq landslide was very likely triggered by a series of accelerated and migratory small earthquakes approaching the nucleation area of the upcoming landslide, thus providing important insights into the failure initiation of massive landslides.

Keywords: nucleation process; landslide; waveform similarity; repeating earthquakes; neighboring earthquakes

check for updates

Citation: Guo, Z.; Hou, X.; Gao, D.; Liu, J. Nucleation Process of the 2017 Nuugaatsiaq, Greenland Landslide. *Forests* **2023**, *14*, 2. https://doi.org/10.3390/f14010002

Academic Editor: Junwei Ma

Received: 15 November 2022
Revised: 13 December 2022
Accepted: 17 December 2022
Published: 20 December 2022

Copyright: © 2022 by the authors. Licensee MDPI, Basel, Switzerland. This article is an open access article distributed under the terms and conditions of the Creative Commons Attribution (CC BY) license (https://creativecommons.org/licenses/by/4.0/).

1. Introduction

Precursory signals preceding catastrophic failure of brittle rocks such as earthquakes and landslides are of great importance in providing critical insights into the nucleation process and, hence, are essential for hazard prediction and mitigation [1–5]. Although foreshocks before significant earthquakes are widely reported and well-recognized [1,4,6,7], seismic precursors prior to a large landslide are rarely documented [8], in part because these signals are small, and unfortunately near-source observation is typically rare. One notable exception is the widely studied 2017 Nuugaatsiaq, Greenland landslide (Figure 1) with abundant seismic precursors (Figure 2) captured by a local seismic station NUUG (Figure 1), at a ~30 km distance [8,9]. This landslide occurred on the evening of 17 June and generated the largest documented tsunami wave (runup height ~90 m) in Greenland to date and caused serious casualties [10].

Although the seismic precursors of the Nuugaatsiaq landslide are of weak amplitudes (Figure 2), their waveforms are highly similar as revealed by both the conventional match filtering (MF) method [8,9] and unsupervised deep learning [11]. Based on the similar waveforms, the seismic precursors are believed to be stick-slip repeating events [8,9,11] and, hence, are interpreted as the manifestation of aseismic slip on the failure surface responsible for the occurrence of the massive Nuugaatsiaq landslide, according to an earlier study [9]. However, a growing body of literature suggests that high waveform similarity may only imply close source areas [1,12–14] and/or similar focal mechanisms [15], but not necessarily repeated ruptures.

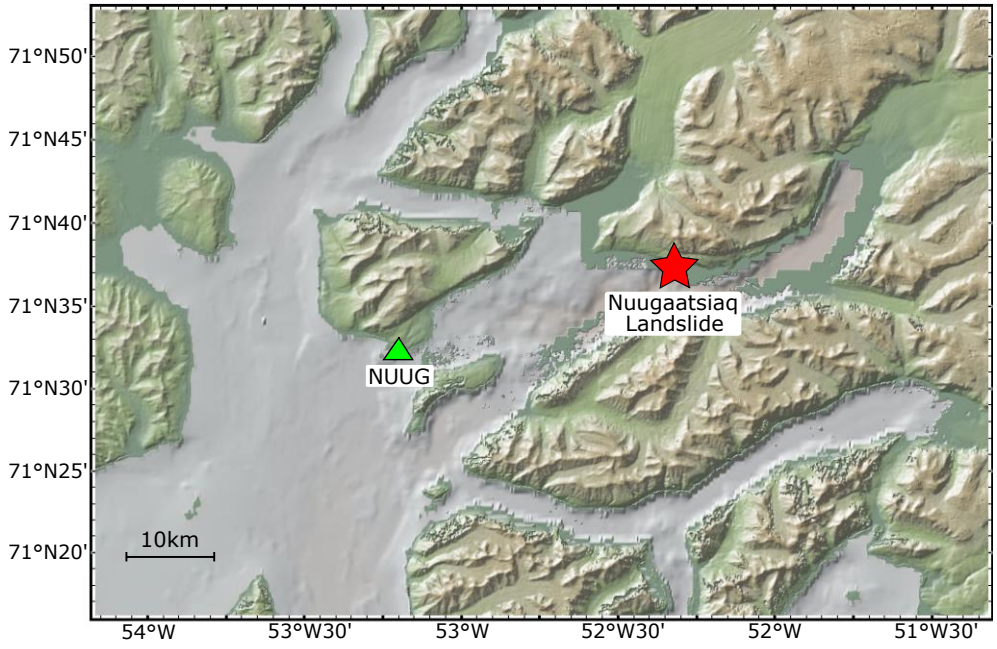


Figure 1. Map of our study area. Red star and lime triangle mark the Nuugaatsiaq landslide and seismic station NUUG, respectively.

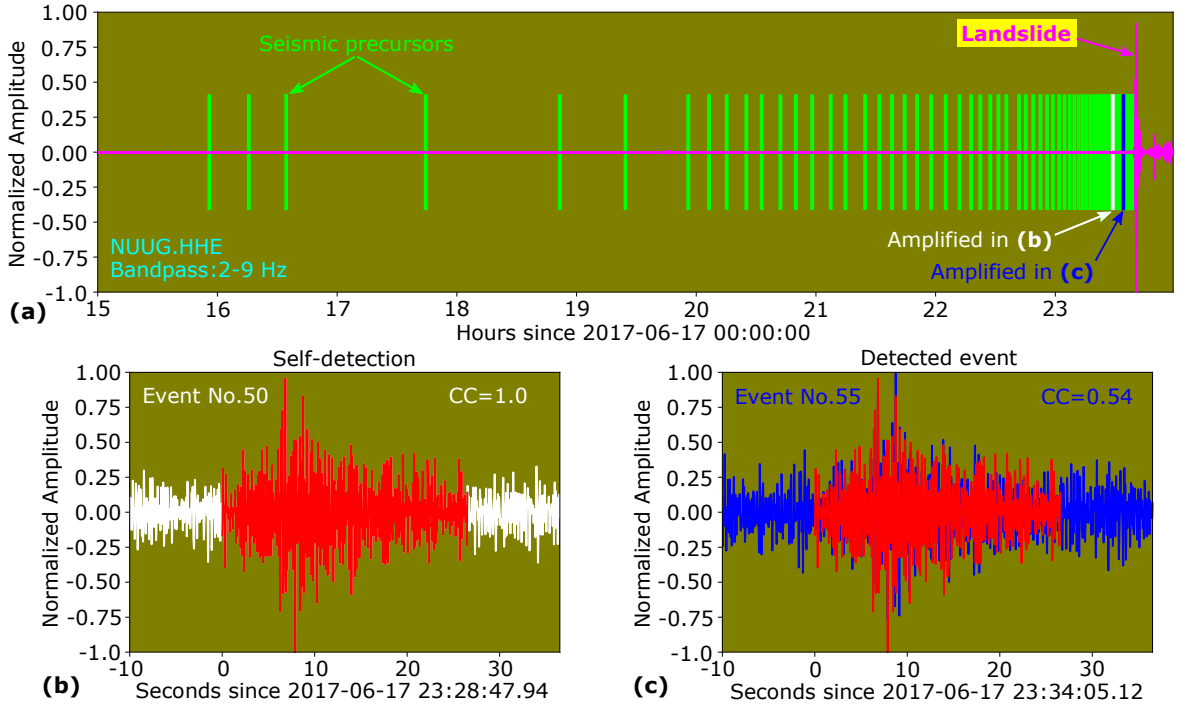


Figure 2. Seismic waveform. (**a**) East component (fuchsia line) of station NUUG. The waveform is normalized and band-pass filtered between 2 and 9 Hz [9]. Colored (lime, white, and blue) vertical bars denote the seismic precursors. (**b**) Self-detection (event No. 50). (**c**) An example of detected event (No. 55). For both (**b**,**c**), the template waveform (event No. 50, red line) is superposed at the location of the best match according to the MFMC method.

Therefore, we revisit the 2017 Nuugaatsiaq landslide with a recently developed match-filtering with multi-segment cross-correlation (MFMC) technique [16]. This technique quantifies the waveform similarity through an averaged cross-correlation coefficient (CC) by equally incorporating the contributions from various segments of the waveforms (see Section 2) and, hence, is very sensitive to the spatial difference between closely spaced

seismic sources [16]. In this study, we first employ the MFMC technique to scan through the 24 h data of station NUUG (Figure 1) before the landslide to construct a reliable dataset of seismic precursors. Then we analyze the temporal evolution of the CC values, waveform amplitudes, and inter-event times of the seismic precursors. Our observations indicate that the 2017 Nuugaatsiaq landslide was very likely triggered by a cascade process with a series of small seismic events approaching the nucleation area of the upcoming landslide, providing important insights into the failure initiation of large landslides.

2. Methods

To identify seismic precursors, we utilize the MFMC technique [16] instead of the conventional MF method which can be severely biased by the presence of large-amplitude phases (e.g., S wave and surface waves) [16–19]. Compared with the conventional MF method with only one segment, the MFMC technique divides the template into a series of consecutive segments during the cross-correlation process. Such a procedure aims to mitigate the influence of the large-amplitude phases and essentially assigns more weights to important low-amplitude phases such as depth phases [20,21] and coda waves [22,23] which contain additional source location information. Hence, the MFMC technique is more reliable in differentiating the source location difference between earthquakes with similar waveforms [16].

In this study, we choose the same template (i.e., event No. 50 in Figure 2b) as a previous study [9] because this event has relatively high signal-to-noise ratio (SNR) (namely, can be visually identified) and more importantly it is isolated from other seismic precursors in the waveform time series [9]. Although the S-P times of the seismic precursors are only about 4.6 s [9], the precursory signals have long surface wave trains (Figure 2b,c) [9,11] due to the shallow source depths. Here we set the template window length (T_{win}) to be 26.5 s covering much of the signal, similar to the choice of prior work [9]. In our MFMC CC calculation, we first band-pass filter the seismic data between 2 and 9 Hz to mitigate the impact of noise [9]. Then we split the template waveform into N_{seg} segments of equal length where N_{seg} is determined by the cycles of the longest period wave ($1/f_{min}$) in the band-pass filtered waveform (i.e., $N_{seg} = T_{win} \times f_{min}$) [16]. Finally, we shift all the segments together one sample point at a time along the continuous waveform. The cross-correlation calculation is performed individually for each segment, and the CC value at each sample point is determined by the average of all segments. Once the computed CC exceeds a certain threshold, an event is declared.

3. Results

In total, we have identified 72 seismic precursors (Figure 2) with the classical detection threshold of 8 times the median absolute deviation (MAD) [24–27] with the MFMC technique. Note the number of identified precursors is slightly fewer than that in prior work [9] as our method only detects events which are located closely to the template event. Overall, the CC values of the detected precursors are low mainly because the precursor signals are of small amplitudes (Figure 2). If we take the template event No. 50 (see Section 2) as the reference, it is quite interesting to see that both the CC values (i.e., waveform similarity) and waveform amplitudes of the seismic precursors initially increase towards the reference event (Figure 3a,b). Previous studies [8,9] hypothesize that the seismic events are repeating earthquakes repeatedly initiated from the same asperity, yet with a growing rupture dimension (Figure 4a). Therefore, the increase of waveform similarity may be due to the rise of signal-to-noise ratio (SNR) [11]. However, this hypothesis does not hold as the CC values and the waveform amplitudes exhibit obviously contrasting trends after the reference event (Figure 3a,b).

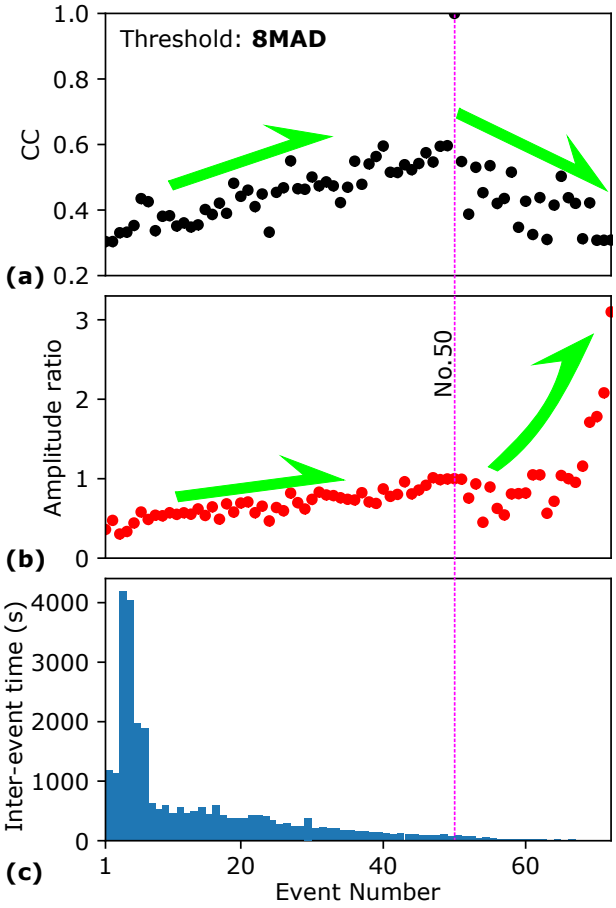


Figure 3. Characteristics of the seismic precursors. (**a**) CC values derived from MFMC. (**b**) Amplitude ratio of the seismic precursors with respect to the reference event No. 50. (**c**) Inter-event times of the seismic precursors. The dashed vertical fuchsia line marks the reference event (No. 50).

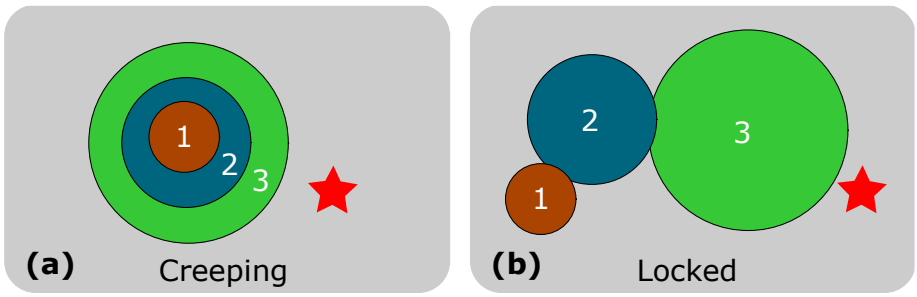


Figure 4. Schematic illustration of the hypothetical nucleation models. (**a**) Aseismic triggering hypothesis [9]. (**b**) Accelerated and migratory triggering hypothesis. In both (**a**,**b**), colored circles represent the seismic precursors; red star marks the nucleation point of the landslide.

Notice that the recurrence times of well-studied repeating earthquakes are widely considered to be on the order of months/years [28–30]. Hence, it is extremally difficult to imagine that the slip surface can repeatedly fail and heal tens of times within only a few hours (Figure 2a). Moreover, recurrence times of true repeating events are nearly constant [28,29] yet the inter-event times of the seismic precursors observed here drop dramatically towards the occurrence of the large landslide (Figure 3c).

Given the similar seismic waveforms, increasing waveform amplitudes, and extremely short and obviously decreasing inter-event times (Figure 3), our observations suggest that the seismic precursors are very likely to be neighboring events progressively triggering larger weak asperities with barely overlapped source areas (Figure 4b). Thus, the overall

trend of CC changes can be fully explained by the migration of the seismic precursors, namely that the CC gets higher when the neighboring events migrate towards the reference event, and vice versa [12,13]. Moreover, both the rising of waveform amplitudes and the shortening of inter-event times can be explained by the accelerating of the inter-event triggering of larger asperities before the landslide, as the sliding surface overall is becoming more and more unstable. Finally, we note that using a detection threshold slightly lower (7.5 MAD) or higher (8.5 MAD) yields similar results and does not change our conclusion.

4. Discussion and Conclusions

Both repeating and neighboring earthquakes are characterized by highly similar waveforms, yet they have totally opposite implications for the nucleation process of catastrophic failure [1,3,12,13]. To unambiguously differentiate these two kinds of events would require sufficient near-source observations to precisely locate the seismic source and calculate the rupture dimension [12,13,31]. With limited data, prior works [8,9,11] have interpretated the seismic precursors as repeating events simply based on waveform similarity. However, recent studies have shown that waveform similarity alone is insufficient to identify true repeating earthquakes [1,12,13] and similar seismic signals with very short inter-event times are commonly taken as neighboring events [12,32].

Although we cannot resolve the source properties of the seismic precursors (e.g., source location, rupture dimension, and stress perturbation) given the single-station waveform data with poor SNR, the observed temporal evolution of the CC values, waveform amplitudes, and inter-event times provides compelling evidence that a series of accelerated and migratory seismic precursors occurred immediately before the 2017 Nuugaatsiaq landslide inherently suggesting a causal relationship likely through a cascade of stress perturbation between neighboring asperities. Notice that our inferred cascade of stress transfer triggering process (Figure 4b) has also been documented to be responsible for some large earthquakes such as the 1999 Mw 7.6 Izmit (Turkey) [1] and 1999 Mw 7.1 Hector Mine (USA) [6]. Our findings bring important insights into the nucleation process of landslides, suggesting that massive landslides may initiate in a similar way as many large earthquakes. However, we note that whether our hypothesis can be generalized to other landslides remains to be tested. Finally, our study highlights the significance of near-source observations in capturing weak precursor signals. Monitoring these tiny signals may not only improve our understanding of the catastrophic failure initiation process but also contribute to hazard preparedness.

Author Contributions: Conceptualization: D.G.; investigation: Z.G., X.H. and D.G.; writing—original draft: Z.G. and X.H.; writing—review & editing: Z.G., X.H., D.G. and J.L. All authors have read and agreed to the published version of the manuscript.

Funding: This research is jointly funded by Open Research Fund Program of Key Laboratory of Metallogenic Prediction of Nonferrous Metals and Geological Environment Monitoring (Central South University), Ministry of Education (Grant No. 2022YSJS16) and National Natural Science Foundation of China (Grant Nos. 42130810 and 42204067).

Data Availability Statement: Waveform data used in this study were downloaded from the Incorporated Research Institutions for Seismology (http://ds.iris.edu/ds/nodes/dmc/, last accessed on 12 July 2022). Seismic data are processed with Obspy [33]. Figures are made with GeoMapApp [34] and Matplotlib [35].

Acknowledgments: We thank two anonymous reviewers for their constructive comments.

Conflicts of Interest: The authors declare no conflict of interest.

References

1. Ellsworth, W.L.; Bulut, F. Nucleation of the 1999 Izmit earthquake by a triggered cascade of foreshocks. *Nat. Geosci.* **2018**, *11*, 531–535. [CrossRef]
2. Tape, C.; Holtkamp, S.; Silwal, V.; Hawthorne, J.; Kaneko, Y.; Ampuero, J.P.; Ji, C.; Ruppert, N.; Smith, K.; West, M.E. Earthquake nucleation and fault slip complexity in the lower crust of central Alaska. *Nat. Geosci.* **2018**, *11*, 536–541. [CrossRef]

3. Gomberg, J. Unsettled earthquake nucleation. *Nat. Geosci.* **2018**, *11*, 463–464. [CrossRef]
4. Zhu, G.; Yang, H.; Tan, Y.J.; Jin, M.; Li, X.; Yang, W. The cascading foreshock sequence of the Ms 6.4 Yangbi Earthquake in Yunnan, China. *Earth Planet. Sci. Lett.* **2022**, *591*, 117594. [CrossRef]
5. Wang, K.; Chen, Q.-F.; Sun, S.; Wang, A. Predicting the 1975 Haicheng earthquake. *Bull. Seismol. Soc. Am.* **2006**, *96*, 757–795. [CrossRef]
6. Yoon, C.E.; Yoshimitsu, N.; Ellsworth, W.L.; Beroza, G.C. Foreshocks and mainshock nucleation of the 1999 M w 7.1 Hector Mine, California, Earthquake. *J. Geophys. Res. Solid Earth* **2019**, *124*, 1569–1582. [CrossRef]
7. Meng, H.; Fan, W. Immediate foreshocks indicating cascading rupture developments for 527 M 0.9 to 5.4 Ridgecrest earthquakes. *Geophys. Res. Lett.* **2021**, *48*, e2021GL095704. [CrossRef]
8. Bell, A.F. Predictability of landslide timing from quasi-periodic precursory earthquakes. *Geophys. Res. Lett.* **2018**, *45*, 1860–1869. [CrossRef]
9. Poli, P. Creep and slip: Seismic precursors to the Nuugaatsiaq landslide (Greenland). *Geophys. Res. Lett.* **2017**, *44*, 8832–8836. [CrossRef]
10. Strzelecki, M.C.; Jaskólski, M.W. Arctic tsunamis threaten coastal landscapes and communities–survey of Karrat Isfjord 2017 tsunami effects in Nuugaatsiaq, western Greenland. *Nat. Hazards Earth Syst. Sci.* **2020**, *20*, 2521–2534. [CrossRef]
11. Seydoux, L.; Balestriero, R.; Poli, P.; de Hoop, M.; Campillo, M.; Baraniuk, R. Clustering earthquake signals and background noises in continuous seismic data with unsupervised deep learning. *Nat. Commun.* **2020**, *11*, 3972. [CrossRef] [PubMed]
12. Gao, D.; Kao, H.; Wang, B. Misconception of waveform similarity in the identification of repeating earthquakes. *Geophys. Res. Lett.* **2021**, *48*, e2021GL092815. [CrossRef]
13. Gao, D. Comprehensive Study of Seismic Waveform Similarity: Applications to Reliable Identification of Repeating Earthquakes and Investigations of Detailed Source Process of Induced Seismicity. Ph.D. Dissertation, University of Victoria, Victoria, BC, Canada, 2021.
14. Cheng, X.; Niu, F.; Silver, P.G.; Horiuchi, S.; Takai, K.; Iio, Y.; Ito, H. Similar microearthquakes observed in western Nagano, Japan, and implications for rupture mechanics. *J. Geophys. Res. Solid Earth* **2007**, *112*, B04306. [CrossRef]
15. Kilb, D.; Rubin, A. Implications of diverse fault orientations imaged in relocated aftershocks of the Mount Lewis, ML 5.7, California, earthquake. *J. Geophys. Res. Solid Earth* **2002**, *107*, ESE 5-1–ESE 5-17. [CrossRef]
16. Gao, D.; Kao, H. Optimization of the match-filtering method for robust repeating earthquake detection: The multisegment cross-correlation approach. *J. Geophys. Res. Solid Earth* **2020**, *125*, e2020JB019714. [CrossRef]
17. Kraft, T.; Deichmann, N. High-precision relocation and focal mechanism of the injection-induced seismicity at the Basel EGS. *Geothermics* **2014**, *52*, 59–73. [CrossRef]
18. Myhill, R.; McKenzie, D.; Priestley, K. The distribution of earthquake multiplets beneath the southwest Pacific. *Earth Planet. Sci. Lett.* **2011**, *301*, 87–97. [CrossRef]
19. Li, L.; Niu, F.; Chen, Q.-F.; Su, J.; He, J. Post-seismic velocity changes along the 2008 M 7.9 Wenchuan earthquake rupture zone revealed by S coda of repeating events. *Geophys. Suppl. Mon. Not. R. Astron. Soc.* **2016**, *208*, 1237–1249. [CrossRef]
20. Ma, S.; Atkinson, G.M. Focal depths for small to moderate earthquakes (m N≥ 2.8) in Western Quebec, Southern Ontario, and Northern New York. *Bull. Seismol. Soc. Am.* **2006**, *96*, 609–623. [CrossRef]
21. Ma, S. Focal depth determination for moderate and small earthquakes by modeling regional depth phases sPg, sPmP, and sPn. Bull. *Seismol. Soc. Am.* **2010**, *100*, 1073–1088. [CrossRef]
22. Snieder, R.; Vrijlandt, M. Constraining the source separation with coda wave interferometry: Theory and application to earthquake doublets in the Hayward fault, California. *J. Geophys. Res. Solid Earth* **2005**, *110*, B04301. [CrossRef]
23. Robinson, D.; Sambridge, M.; Snieder, R. A probabilistic approach for estimating the separation between a pair of earthquakes directly from their coda waves. *J. Geophys. Res. Solid Earth* **2011**, *116*, B04309. [CrossRef]
24. Shelly, D.R.; Beroza, G.C.; Ide, S. Non-volcanic tremor and low-frequency earthquake swarms. *Nature* **2007**, *446*, 305–307. [CrossRef] [PubMed]
25. Shelly, D.R.; Skoumal, R.J.; Hardebeck, J.L. S/P Amplitude Ratios Derived from Single-Component Seismograms and Their Potential Use in Constraining Focal Mechanisms for Microearthquake Sequences. *Seism. Rec.* **2022**, *2*, 118–126. [CrossRef]
26. Thomas, A.M.; Bostock, M.G. Identifying low-frequency earthquakes in central Cascadia using cross-station correlation. *Tectonophysics* **2015**, *658*, 111–116. [CrossRef]
27. Kurihara, R.; Obara, K.; Takeo, A.; Maeda, T. Migration of deep low-frequency tremor triggered by teleseismic earthquakes in the southwest Japan Subduction Zone. *Geophys. Res. Lett.* **2018**, *45*, 3413–3419. [CrossRef]
28. Uchida, N.; Matsuzawa, T.; Ellsworth, W.L.; Imanishi, K.; Shimamura, K.; Hasegawa, A. Source parameters of microearthquakes on an interplate asperity off Kamaishi, NE Japan over two earthquake cycles. *Geophys. J. Int.* **2012**, *189*, 999–1014. [CrossRef]
29. Abercrombie, R.E. Stress drops of repeating earthquakes on the San Andreas fault at Parkfield. *Geophys. Res. Lett.* **2014**, *41*, 8784–8791. [CrossRef]
30. Bohnhoff, M.; Wollin, C.; Domigall, D.; Küperkoch, L.; Martínez-Garzón, P.; Kwiatek, G.; Dresen, G.; Malin, P.E. Repeating Marmara Sea earthquakes: Indication for fault creep. *Geophys. J. Int.* **2017**, *210*, 332–339. [CrossRef]
31. Waldhauser, F.; Schaff, D.P. A comprehensive search for repeating earthquakes in northern California: Implications for fault creep, slip rates, slip partitioning, and transient stress. *J. Geophys. Res. Solid Earth* **2021**, *126*, e2021JB022495. [CrossRef]

32. Li, L.; Chen, Q.f.; Niu, F.; Su, J. Deep slip rates along the Longmen Shan fault zone estimated from repeating microearthquakes. *J. Geophys. Res. Solid Earth* **2011**, *116*, B09310. [CrossRef]
33. Beyreuther, M.; Barsch, R.; Krischer, L.; Megies, T.; Behr, Y.; Wassermann, J. ObsPy: A Python toolbox for seismology. *Seismol. Res. Lett.* **2010**, *81*, 530–533. [CrossRef]
34. Ryan, W.B.; Carbotte, S.M.; Coplan, J.O.; O'Hara, S.; Melkonian, A.; Arko, R.; Weissel, R.A.; Ferrini, V.; Goodwillie, A.; Nitsche, F. Global multi-resolution topography synthesis. *Geochem. Geophys. Geosyst.* **2009**, *10*, Q03014. [CrossRef]
35. Hunter, J.D. Matplotlib: A 2D graphics environment. *Comput. Sci. Eng.* **2007**, *9*, 90–95. [CrossRef]

Disclaimer/Publisher's Note: The statements, opinions and data contained in all publications are solely those of the individual author(s) and contributor(s) and not of MDPI and/or the editor(s). MDPI and/or the editor(s) disclaim responsibility for any injury to people or property resulting from any ideas, methods, instructions or products referred to in the content.